The potassium channel: Structure, selectivity and diffusion

T. W. Allen[a)]
Protein Dynamics Unit, Department of Chemistry, Australian National University, Canberra, Australian Capital Territory 0200, Australia

A. Bliznyuk and A. P. Rendell
Supercomputing Facility, Australian National University, Canberra, Australian Capital Territory 0200, Australia

S. Kuyucak
Department of Theoretical Physics, Research School of Physical Sciences, Australian National University, Canberra, Australian Capital Territory 0200, Australia

S.-H. Chung
Protein Dynamics Unit, Department of Chemistry, Australian National University, Canberra, Australian Capital Territory 0200, Australia

(Received 14 December 1999; accepted 8 February 2000)

We employ the entire experimentally determined protein structure for the KcsA potassium channel from *Streptomyces lividans* in molecular dynamics calculations to observe hydrated channel protein structure, ion solvation, selectivity, multiple ion configurations, and diffusion. Free energy perturbation calculations display a significant ion discrimination of ~ 9 kT in favor of the larger K^+ ion. The protein forming the channel is very flexible yet is unable to fully solvate the Na^+ ion because of its smaller size and large solvation energy. There is evidence that acidic and basic sidechains may dissociate in the presence of multiple K^+ ions to explain experimental ion density maps. K^+ diffusion is found to vary from approximately 10%–90% of bulk, supporting the high channel currents observed experimentally. © *2000 American Institute of Physics.* [S0021-9606(00)50617-5]

I. INTRODUCTION

In this article we examine the structure, thermodynamics, and diffusion of ions within the KcsA potassium channel. We employ coordinates obtained by 3.2 Å resolution x-ray diffraction studies of the potassium channel from *Streptomyces lividans*[1] in molecular dynamics (MD) calculations. The aim is to further our understanding of ion permeation and selectivity within this complex biological ion channel. Understanding the mechanisms behind the operation of this channel is important because of the channel's role in neuronal signaling, and its existence in all biological organisms.

The potassium channel has received considerable experimental attention recently, especially since the publication of the KcsA potassium channel structure.[1] Studies of gating mechanisms, involving structural rearrangements,[2,3] *p*H dependence,[4] and experiments with similar potassium channels[5–7] help us understand channel permeation and selectivity. While much about the potassium channel is being revealed, MD simulation of the hydrated channel protein seems the only way to unveil microscopic details such as intrapore ion–ion interactions, ion solvation environment and energy, and localized ion diffusion coefficients. MD studies of model cylindrical channels,[8–10] small bacterial pores such as gramicidin A[11] and complex proteins like sodium and nAChR channels[12,13] and the large OmpF porin[14] exist. However, to date, MD investigation into the potassium channel is limited to a simplified model channel,[15] where only a small fraction representing the selectivity filter of the protein is treated explicitly. This simplified model has shed some light on ion permeation and selectivity mechanisms with a minimal computational effort. However, a MD study involving the entire channel protein is the only way to extract important microscopic details with minimal model dependence. The simulations reported here involve a combined total of 63 ns requiring over 2 CPU years on a Silicon Graphics Power Challenge R10000.

The aim of this MD study is to provide an improved channel description that reproduces and reinforces experimental findings in the KcsA potassium channel. The most important property of the potassium channel is its ability to selectively conduct K^+ ions with a high throughput (10 pA[16]) while suppressing that of Na^+ by at least a factor of 10^4. Thus there must be a free energy barrier for the Na^+ ion relative to the K^+ ion that explains this selectivity margin, yet the energy profile, lateral ion positions, and levels of diffusion coefficient should be such that a high K^+ ion current is still possible. Ion positions within the outer channel are suggested by ion difference maps,[1] and multiple ion configurations from MD simulation should approximately reproduce these regions of high ion density. Water positions have not been resolved experimentally, therefore, MD coordinates provide a useful means for determining the ability of water to penetrate regions of the pore.

We first detail our model and then describe the structure

a)Electronic mail: Toby.Allen@anu.edu.au

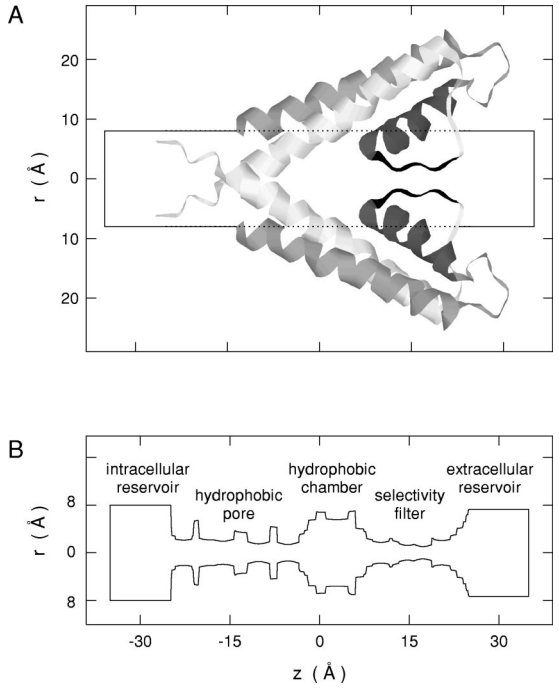

FIG. 1. (A) Initial potassium channel protein structure and reservoir definitions. The outer helices and turrets (light gray ribbons), pore helices (dark gray ribbons), selectivity filter (narrow black ribbons), and inner helices (white ribbons) for two subunits of the tetramer are drawn. (B) The initial pore radius (accounting for van der Waals radii) is shown. Indicated are the selectivity filter, hydrophobic chamber, hydrophobic pore, and the intracellular and extracellular reservoirs.

of the equilibrated solvated protein and the influence of applied restraining potentials. Next we report protein potential calculations that are used to analyze the effect of charged amino acid residues. We then describe ion coordination, potential energy profiles, and provide a free energy perturbation profile to give some measure of the extent of ion discrimination within the model channel. Finally, we discuss water properties, multiple ion configurations, and give estimates of the ion diffusion coefficient within the channel. This comprehensive set of results should aid our understanding of the microscopic properties and conduction mechanisms underlying this important biological channel.

II. MODEL SYSTEM

Figure 1(A) illustrates the model KcsA potassium channel protein structure, where two subunits of the tetramer of peptide chains which form the channel are shown. Each subunit consists of 158 signature amino acid residues, of which 97 have been determined by x-ray diffraction.[1] The entire experimentally determined protein structure is employed such that in total the model system consists of 396 residues, including terminal groups.[17] Initial coordinates, described by Doyle *et al.*,[1] are taken from the Protein Data Bank *1bl8* set. The amino acid sequence is divided into segments of interest in Table I.

The channel radius profile (accounting for atomic size) for the initial protein coordinates, in the absence of any water, is shown in Fig. 1(B). The channel extends from approximately -25 to 25 Å. The selectivity filter region adjacent to

TABLE I. KcsA signature amino acid sequence. The residues within each subunit of the experimentally determined potassium channel protein structure are divided into segments.

Segment	Residues	
N-terminal	22	CH_3-CO-
Outer helix	23–61	ALHWRAAGAATVLLVIVLL-AGSYLAVLAERGAPGAQLIT
Pore helix	62–74	YPRALWWSVETAT
Selectivity filter	75–79	TVGYG
Inner helix	80–119	DLYPVTLWGRCVAVVVMVA-GITSFGLVTAALATWFVGREQ
C terminal	120	CH_3-NH-

the extracellular space extends from $z=8$ to 22 Å with a mean radius of ~ 1.4 Å. This region is lined with carbonyl and hydroxyl oxygen atoms making it hydrophilic in nature. There is a large hydrophobic chamber region on the intracellular side of the selectivity filter extending from $z=-2$ to 8 Å with an average radius of ~ 6 Å. The field of the pore helix dipole,[18] in combination with the –COOH terminal (threonine T_{74} residue) and the abundance of water in the cavity, is thought to stabilize ions and overcome the dielectric barrier within this hydrophobic segment.[19]

The long thin hydrophobic pore formed by the inner helices leading to the intracellular space extends from -20 to -2 Å with a minimum radius of 1.5 Å. Spin labeling and electron paramagnetic resonance experiments suggest that this conformation may correspond to a closed state[2,3] and that the conducting pore may be much wider. However, since the dimensions of the hydrophobic pore are not likely to influence ion selectivity, and the pore may be made arbitrarily large by applying forces to the inner helicies, we consider only the experimentally determined configuration. The channel entrances ($-25<z<-20$ and $22<z<25$ Å) and the reservoirs ($25<|z|<35$ Å) provide bulklike environments and useful reference points. Reservoirs are formed by a harmonic bounding cylinder of radius 8 Å[20] acting only on water oxygen atoms and ions. Periodic boundaries are applied at $|z|=35$ Å, enforced by a single image placed at each end of the 70-Å-long segment in the axial direction.

The water in the reservoirs is sampled from equilibrated bulk water in the range $|z|>25$ Å with radius less than 8 Å such that the mean water density is approximately 1 g/cm^3. The water within the channel ($|z|\leqslant 25$ Å) is taken from equilibrated coordinates with a simplified model of the potassium channel.[15] This simplified model employs a Lennard-Jones (LJ) 5-3 potential at the pore lining throughout, except for the narrow hydrophilic selectivity filter region where protein is treated explicitly. Any water molecule with an oxygen atom center closer than 2 Å to a protein atom center is moved away or into a reservoir. Water coordinates inside and outside the channel are then combined. The number of water molecules remaining after this procedure is 210.

III. MOLECULAR DYNAMICS AND POTENTIAL MODELS

MD simulations are performed using the CHARMM v.25 code.[21] A time step of 1 fs is used in the simulations with the Verlet algorithm. Velocity rescaling at 1 ps intervals leads to

temperatures 298±1 K. Coordinates are saved each 0.1 ps for trajectory analysis. A switched force cutoff for electrostatic interactions and a switched potential cutoff for LJ 12-6 interactions are applied to atoms at 12 Å, slowly turned off from 8 Å.[22] The use of a 12 Å cutoff should prevent detrimental effects on diffusion.[23,24] Nonbonded interaction lists are recorded out to 13 Å and are updated at 5–10 fs intervals.

The extended simple point charge (SPC/E) water model[25] is used in all simulations because of its ability to accurately reproduce bulk water and ionic properties. SPC/E LJ 12-6 parameters provided by Berendsen, Grigera, and Straatsma[25] are combined with ion–water parameters[26,27] and ion–ion parameters.[28] Ion–protein LJ 12-6 interactions are determined by CHARMM with standard combination rules.

The united atom (CHARMM19)[29] and all hydrogen (CHARMM22)[30] parameter sets are compared to see if explicit simulation of hydrogen atoms have any effect on channel protein and water structure. For example, CH_3- is represented by four atoms in CHARMM22, while CHARMM19 requires just one atom. After adding the necessary hydrogen atoms using appropriate bond lengths and angles, the total number of protein atoms increases from 3504 to 5916. Equilibrated structures in the presence of water are found to be very similar with the SPC/E water molecules hydrating the pore equally well in both cases. Thus the inclusion of all hydrogen atoms does not appear to be necessary for this potassium channel study, and the additional computational cost can be avoided.

The TIP3P model[31] and its flexible version is found to be unable to solvate the hydrophilic interior of the selectivity filter region, even in the presence of a K^+ ion. This would result in energy barriers for a K^+ ion attempting to traverse the channel. We note that the failure of the TIP3P water model to hydrate the selectivity filter is observed with both united and all hydrogen parameter sets, despite the fact that the all hydrogen CHARMM22 parameters are designed particularly for use with the TIP3P model. The TIP3P and SPC/E water models possess very similar atomic partial charges, dipole moments, and Lennard-Jones forces, but have contrasting geometrical parameters. We conjecture that the larger HOH angle of 109.47° for SPC/E water (in comparison to 104.52° for TIP3P), and the increased OH bond length of 1 Å (in comparison to 0.957 Å for TIP3P) aid the bridging of carbonyl groups across the narrow selectivity filter pore. Stable hydrogen bond networks seem to be unattainable with the TIP3P model.

IV. SHAPE OF THE HYDRATED CHANNEL

The structure of the potassium channel protein and water after 150 ps of equilibration with a weak set of constraints[32] is displayed in Fig. 2(A). It is clear from this figure that the water is solvating the entire pore of this channel, including the narrow hydrophobic region toward the intracellular space. Figure 2(B) displays the time averaged minimum effective pore radius calculated from the last 100 ps of dynamics. The pore radius in the hydrophobic region of the channel is highlighted in Fig. 2(C). There has been little widening of the long hydrophobic region of the channel compared to the original coordinates, despite the reduced constraint strength.

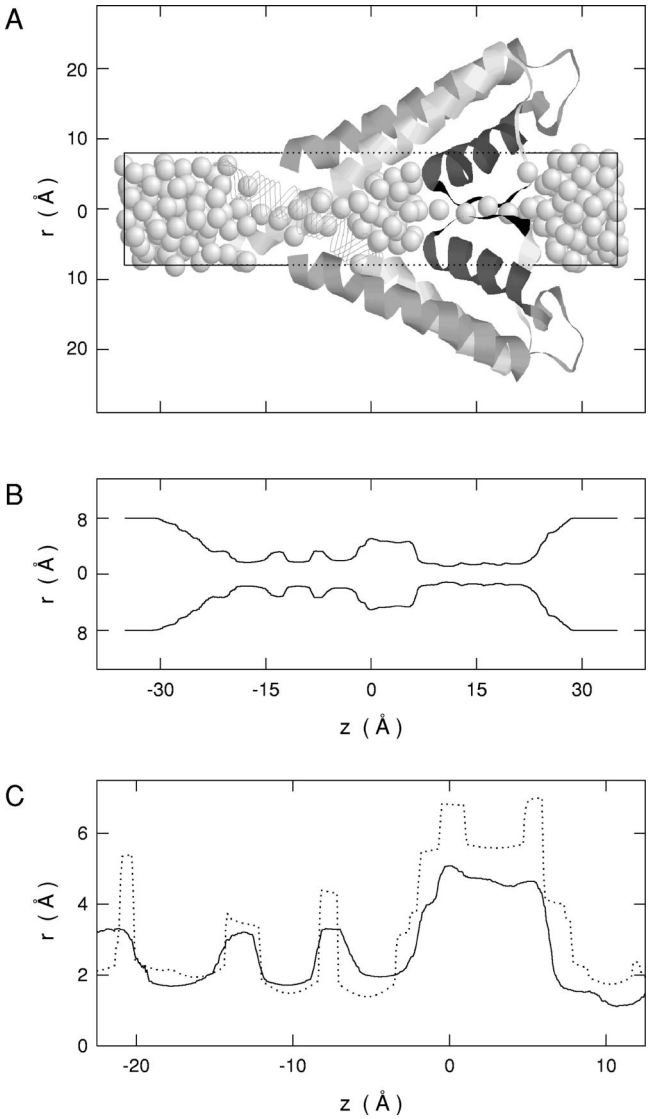

FIG. 2. (A) Hydrated potassium channel structure after 150 ps of dynamics. The intracellular half of one inner helix has been replaced by thin strands to reveal the water positions within the long hydrophobic pore region. (B) The time averaged pore radius (accounting for van der Waals radii) is shown. (C) Comparison of equilibrated (solid line) and initial (dotted line) pore radii in the hydrophobic regions.

Carbonyl and hydroxyl oxygen atoms reside at least 1 Å from the pore lining in the region $-25 \leqslant z \leqslant 8$ Å. Thus this region has maintained its hydrophobic nature after equilibration.

V. CONSTRAINTS

In the present study, the lipid bilayer is not explicitly simulated, instead protein–lipid interactions are represented by some restraining potentials. We summarize results from our survey of restraining potential strengths here. A single K^+ or Na^+ ion is placed at key positions within the hydrated channel, and at a reference point ($z=30$ Å) in the extracellular reservoir. The ion is held at each z value with a harmonic force constant of 20 kT/Å^2, but is free to move in the xy plane. To ensure thorough equilibration, simulation periods of 250–650 ps are used. Simulations are performed

TABLE II. Effect of restraining potentials on ion energies. Ion potential energies with respect to the reservoir (ΔE), and free energy perturbation measurements for the transformation $K^+ \rightarrow Na^+$ with respect to the reservoir ($\Delta\Delta A$) are given for a range of restraining potentials. Values are provided for two test positions: $z=16.0$ Å and $z=20.4$ Å. The energies are listed against the strength of constraints (K) on inner and outer helix α-carbon atoms. Errors are ± 1 standard error of means in potential energies, and are taken from hysteresis values for the free energy perturbations.

z (Å)	K (kT/Å^2)	ΔE_{K^+} (kT)	ΔE_{Na^+} (kT)	$\Delta\Delta A_{K^+\rightarrow Na^+}$ (kT)
16.0	0	-19.1 ± 5.5	-0.3 ± 4.9	3.2 ± 0.5
	5	-8.1 ± 3.1	-5.2 ± 4.1	8.0 ± 1.1
	10	-16.0 ± 3.1	-6.2 ± 4.9	5.9 ± 2.8
	15	-16.6 ± 2.8	2.7 ± 4.5	6.0 ± 1.9
	20	-28.0 ± 3.8	-11.4 ± 4.1	6.4 ± 0.7
20.4	0	-12.4 ± 4.8	-8.7 ± 7.7	⋯
	5	-10.9 ± 2.8	-0.5 ± 4.5	⋯
	10	-9.1 ± 3.1	-9.1 ± 3.3	⋯
	15	-11.3 ± 3.1	-2.2 ± 4.5	⋯
	20	-13.4 ± 3.8	2.9 ± 5.9	⋯

with various strength restraining potentials applied to the protein to observe their influence on ion discrimination. Harmonic potentials, applied to α-carbon atoms on inner and outer helices, range from 0 to 20 kT/Å^2.

Total system energies cannot be compared between simulations because of large variations, even after long equilibration periods due to motions of sidechains away from the pore. For example, a tryptophan sidechain on the inner helix near $z=-20$ Å has been observed moving 6 Å in 3 ps (200 m/s) resulting in a $\sim$200 kT reduction in the total system energy. The effect of this on the pore radius is less than 0.1 Å outwards motion restricted to the region $-23\leqslant z\leqslant -19$ Å. Thus, although such a large drop in system energy could suggest lack of equilibration, the change has little influence on important channel properties, and most important, no influence on the ion energy margins within the selectivity filter.

Table II lists K^+ and Na^+ ion potential energies at positions near the center ($z=16.0$ Å) and extracellular end ($z=20.4$ Å) of the selectivity filter for various constraint strengths. With the exception of 5 kT/Å^2 where the difference is within the error range, a significant energy margin between the Na^+ and K^+ ions exists at $z=16.0$ Å, irrespective of the strength of applied constraints. We note that large margins are also seen when constraints are only applied to the inner or outer helices. In fact, a large difference exists in the absence of any applied constraints. Large potential energy differences are also seen at $z=20.4$ Å, where only for constraint strengths 0 and 10 kT/Å^2 are the differences within the error range.

Free energy perturbations ($K^+ \rightarrow Na^+$) with respect to the extracellular reservoir, described in Sec. IX, are also provided for $z=16.0$ Å in Table II. The free energy perturbation calculations also reveal a preference for the K^+ ion over Na^+. High perturbation values of 6–8 kT emerge for all nonzero constraints. The lower value obtained in the absence of any constraints is not significant since it is difficult to maintain the protein geometry under such conditions for long simulation periods (800 ps).

TABLE III. Positions of charged amino acids from equilibrated sample coordinates. Mean positions of carboxyl oxygens on glutamic acid (E) aspartic acid (D) residues, and of the guanidine carbon on arginine (R) residues are listed. These are centers of high excess charge concentration. Residues have been collected into likely pairs.

$(\overline{r}, \overline{z})$ (Å)
E^-_{51} (16.7, 22.9), R^+_{52} (23.4, 25.5)
D^-_{80} (9.2, 21.2), R^+_{64} (10.7, 25.2)
E^-_{71} (6.1, 16.6), R^+_{89} (11.2, 19.5)
R^+_{27} (19.4, -13.9)
E^-_{118} (3.6, -22.3), R^+_{117} (11.9, -22.2)

As further evidence of the lack of involvement of applied restraining potentials on ion discrimination we examine the constraint energy contributions to the total system energy. The total constraint energy (excluding ion constraint) in the presence of a Na^+ ion at $z=16.0$ Å with respect to that for a K^+ ion at the same position for constraints 5, 10, 15, and 20 kT/Å^2 is -1.8 ± 1.2, 3.3 ± 2.2, 0.2 ± 2.4, and 2.0 ± 2.7 kT, respectively. Since there is no consistent positive contribution of the constraint energy to the system energy when a K^+ is replaced by a Na^+ ion, there should be little contribution to ion discrimination. This information permits us to choose any strength of constraint within the tested range. We choose 20 kT/Å^2 to maintain stability of the entire structure over long simulation periods. Similar strength restraining potentials have been used in model nAChR studies.[33]

VI. EFFECT OF CHARGED AMINO ACIDS

We examine the effect of charged residues by comparing protein potential profiles obtained from MD trajectories with neutral and charged amino acids. In charged protein simulations all glutamic and aspartic acid residues carry a unit negative charge ($-e$) while the basic arginine residues have unit positive charge ($+e$). Atomic partial charges for neutral acidic and basic residues have been taken from Lazaridis and Karplus.[34] Equilibrated positions of charged residues in the first subunit of the protein are listed in Table III. Near the extracellular entrance and selectivity filter region there are three pairs of oppositely charged residues, while near the intracellular entrance there is one pair that is likely to stabilize cations in the pore. In the narrow hydrophobic pore region there exists one unpaired positive charge per subunit that could destabilize cations.

Figure 3 compares electrostatic potential profiles for neutral and charged proteins along the channel axis. The values plotted are contributions from protein atoms only with no long-range potential truncation. Water contributions are excluded because of the considerable noise introduced by water atoms approaching close to profile grid points. Rather than assign an arbitrary dielectric constant to the channel water, we plot the potential for a relative permittivity of 1, acknowledging that channel water will attenuate these electrostatic potentials. The influence of positively charged arginine residues, not accompanied by any acidic residues, near $z=-14$ Å is to raise the potential in the narrow hydrophobic pore region by $\sim$1.9 V (or approximately 74 kT for a unit charge), despite their distance from the pore. Although much

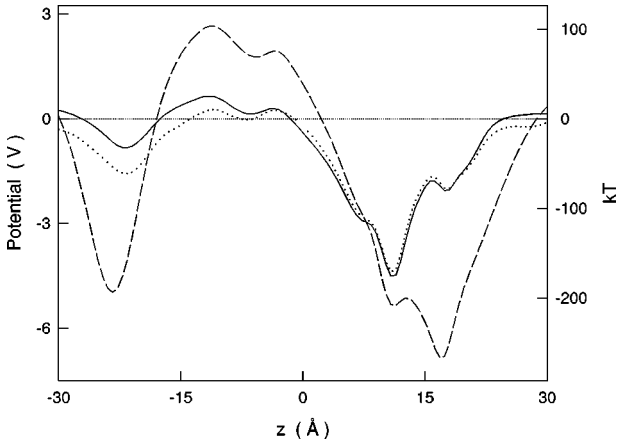

FIG. 3. Protein potential profile: Time averaged electrostatic potential due to the protein along the z axis is shown. The solid curve represents the simulations with neutral amino acids while the dashed curve represents the simulation with charged arginine, glutamic acid, and aspartic acid residues. The dotted curve shows the potential profile for the neutral protein calculated with a switched force long-range cutoff. The left-hand vertical axis displays the potential in V while the right-hand axis provides energy units corresponding to a unit charge e.

of this potential may be shielded by water, it is fairly certain that the $+4e$ charge in this region would prevent conduction. Near the intracellular entrance region we observe a dramatic fall in protein potential contributions (by approximately 4.2 V or 162 kT) when residues become charged. In the selectivity filter and extracellular entrance regions the potential falls by as much as 4.8 V (187 kT). The generation of a deep second potential well near $z=17$ Å within the filter region could have considerable influence on multiple ion configurations and permeation mechanisms.

In all remaining simulations only the neutral protein is considered. We comment later on the possible effect of charged residues on ion energies and multiple ion configurations. In MD simulations an integrated switched force cutoff is applied to electrostatic interactions. Figure 3 also shows the potential profile for the neutral protein with this cutoff applied. The effect of the truncation is negligible except near the intracellular entrance, where a ~ 0.7 V drop in potential is observed.

VII. ION POTENTIAL ENERGY PROFILES

A single K^+ or Na^+ ion is placed at one of 19 different positions along the channel axis and simulation is carried out for 150 ps. Ion potential energies,[35] and separate water and protein contributions, are plotted in Fig. 4 for K^+ (A) and Na^+ (B) ions. These profiles clearly depict the remarkable ability of the protein to provide a stabilizing potential as water molecules are stripped away from each ion in the selectivity filter. For the K^+ ion the protein accounts for nearly all of the ion's solvation energy within the range $10 \leqslant z \leqslant 16$ Å. As a result of the strong protein involvement, the K^+ ion experiences low potential energies throughout the selectivity filter.

Potential energy differences with respect to the reservoir are plotted in Fig. 5 for both ion types. The K^+ ion potential energy is as low as -39.1 ± 2.7 kT with respect to reservoir. The potential energy margin between Na^+ and K^+ ions is as high as 28 ± 4.6 kT in the selectivity filter. We note that ion potential energies do not include all of the components necessary to describe channel permeation. Changes in the protein energy in response to the introduction of an ion could also play a significant role. For example, the small positive relative potential energy for Na^+ near $z=20$ Å would not be sufficient to explain the inability of Na^+ ions to enter the

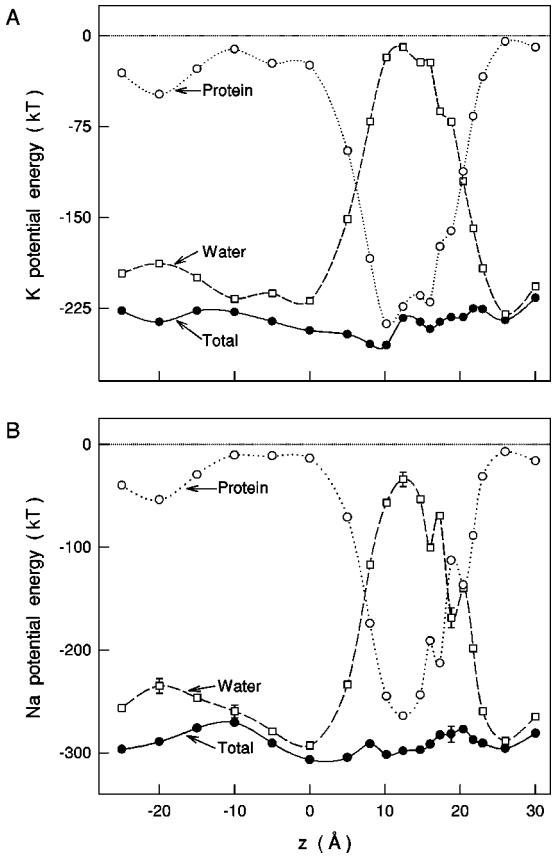

FIG. 4. Ion interaction energies of K^+ (A) and Na^+ (B) ions: Total interaction energies with surroundings are drawn as solid curves (closed circles), interaction energies with water as dashed curves (open squares), and the interaction energy with the protein as dotted curves (open circles). Error bars are ± 1 standard error of means and are only shown if larger than the point symbol.

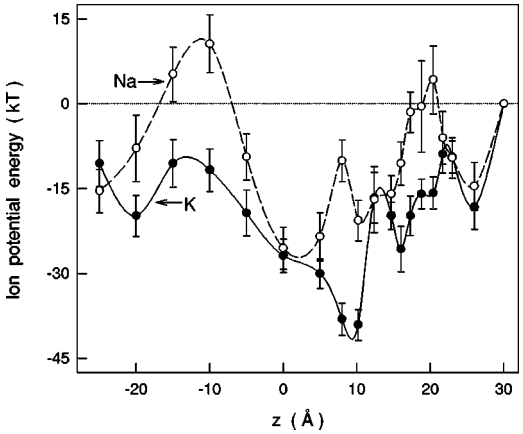

FIG. 5. Total ion potential energies with respect to the reservoir values are drawn for K^+ (solid curve, closed circles) and Na^+ (dashed curve, open circles). Error bars are ± 1 standard error of means.

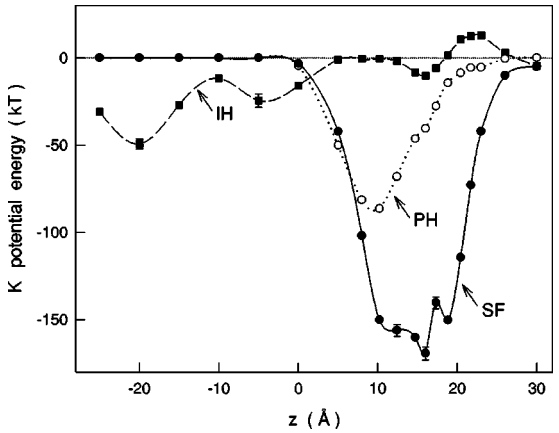

FIG. 6. Protein contributions to the K^+ ion potential energy: The curves labeled SF, PH, and IH represent the contributions from the selectivity filter (solid curve, closed circles), pore helix (dotted curve, open circles), and inner helix (dashed curve, closed squares), respectively. Error bars are ± 1 standard error of means and are not shown if they are too small to view.

channel from the exterior. In Sec. IX we measure the free energy margin between K^+ and Na^+ ions. The inclusion of entropy components should provide a better measure of the ability of the channel to discriminate between these ions. Nevertheless, Fig. 5 gives an indication of the relative stabilities of the two ions at each position within the channel and will help explain multiple ion configurations in Sec. XI.

Within the narrow hydrophobic segment of the channel the Na^+ ion potential energy is 10.6 ± 5.1 kT above the reference value, approximately 22 kT less stable than the K^+ ion. This narrow hydrophobic pore will exclude Na^+ ions from the channel, but will not prevent K^+ ions from passing. Since Na^+ ions are known to enter the intracellular mouth of the channel and block K^+ ion permeation,[36] the presence of such a barrier suggests that the conducting channel should have a wider hydrophobic pore, in agreement with experimental gating studies.[2,3]

Figure 6 shows the separate contributions of segments of the protein to the potential energy of the K^+ ion. The pore helix potential energy contribution reaches a minimum of -86.5 ± 1.2 kT at $z \approx 10$ Å, at the intracellular side of the selectivity filter. Although the dipole of the pore helix remains directed toward the origin, the contribution of the pore helix is a maximum near $z \approx 10$ Å because of the stabilizing effect of the T_{74} carbonyl oxygen atom at the base of the pore helix. Note that the contribution of the selectivity filter protein to the stabilizing potential in the wide chamber region is just as significant as that of the pore helix.

In the simplified model potassium channel[15] the pore helices are represented by electric dipoles with charges $\pm 0.6 \times 10^{-19}$ C, leading to an energy well of ~ 60 kT for a K^+ ion within the hydrophobic cavity. This well is seen to be about 40 kT in the present study. This suggests the use of smaller charges of approximately $\pm 0.5 \times 10^{-19}$ C (based on the well depth study of Allen, Kuyucak, and Chung[15]) for the simple model dipoles to better represent the pore helices.

The inner helix provides a -49.4 ± 2.8 kT stabilizing potential energy near $z = -20$ Å, with some influence over the entire hydrophobic region. A small positive, destabilizing contribution of $+12.8 \pm 0.8$ kT is made by the inner helix near the extracellular entrance of the selectivity filter. This contribution is evident as a bump in the total K^+ ion potential energy in Fig. 5. The contribution of the outer helix is very small throughout the channel, varying from approximately -0.4 to 1.5 kT.

VIII. ION COORDINATION

In order to explain how the potential energy margins arise within the channel we first examine bulk solvation. We have determined that within the reservoir region, the total potential energy of the K^+ ion is -216.6 ± 2.0 kT, of which -173.1 ± 1.7 kT comes from the first hydration shell and the remaining -43.5 ± 2.6 kT from outer hydration shells. The total potential energy of the Na^+ ion is -281.3 ± 2.3 kT and the first shell contribution is -232.2 ± 1.0 kT, leaving -49.0 ± 2.5 kT for outer shells to contribute. If both ions were stripped to first hydration shells only, there would be a relative barrier of 5.5 ± 3.6 kT for the Na^+ ion in comparison to the K^+ ion. Thus, the large potential energy margins observed (Fig. 5) must come from inadequate formation of the first solvation shell of Na^+. Because the first shell contribution of Na^+ is much larger than that of K^+ (by ~ 60 kT), small deviations from optimal bulklike first shell solvation will have a more drastic effect on Na^+ stability. For example, if one were to artificially shift the bulk first hydration shells of K^+ and Na^+ ions outwards by 0.1 Å,[37] the contribution of the first shell to the ions' potential energies would rise by 9.9 ± 2.2 and 16.3 ± 1.3 kT, respectively, resulting in a 6.4 ± 2.5 kT energy margin.

Radial distribution functions (RDFs) for K^+ and Na^+ ions have been calculated at each position within the channel pore. Figure 7 shows the positions of the first maxima in the ion–water oxygen and ion–protein oxygen RDFs for K^+ (A) and Na^+ (B) ions. The bulk first shell RDF properties are listed in Table IV as a comparison. Both ion types experience a close-packed first solvation shell throughout the channel and reservoirs, except at some positions within the selectivity filter. Averaging the difference between first ion–protein and bulk ion–water oxygen maxima over the range $8 \leqslant z \leqslant 21.7$ Å results in a mean gap of 0.03 ± 0.02 Å for the K^+ ion, and 0.10 ± 0.02 Å for the Na^+ ion. The gap observed for Na^+ arises because protein oxygens are unable to move in toward the ion enough to mimic water oxygens. Within bulk, the first Na^+ shell (density peaking at 2.32 Å) resides approximately 0.44 Å closer to the ion than does that for the K^+ ion (at 2.76 Å). The protein oxygens may be held away from the Na^+ ion by internal protein restoring forces which prohibit large flexible motions, by external electrostatic and van der Waals interactions of the filter protein with the pore helix, by repulsive Coulomb forces acting between carbonyls on opposite sides of the pore, or may be pushed away from the small ion by the larger hydrating water molecules either side of the ion. Because K^+ has a Pauling radius 1.33 Å, approximately equal to that of a water molecule (~ 1.4 Å), little bending of the protein chain would be required to permit good solvation. However, a smaller Na^+ ion (with Pauling radius 0.95 Å) at the same position would require large inward motions of central oxygens.

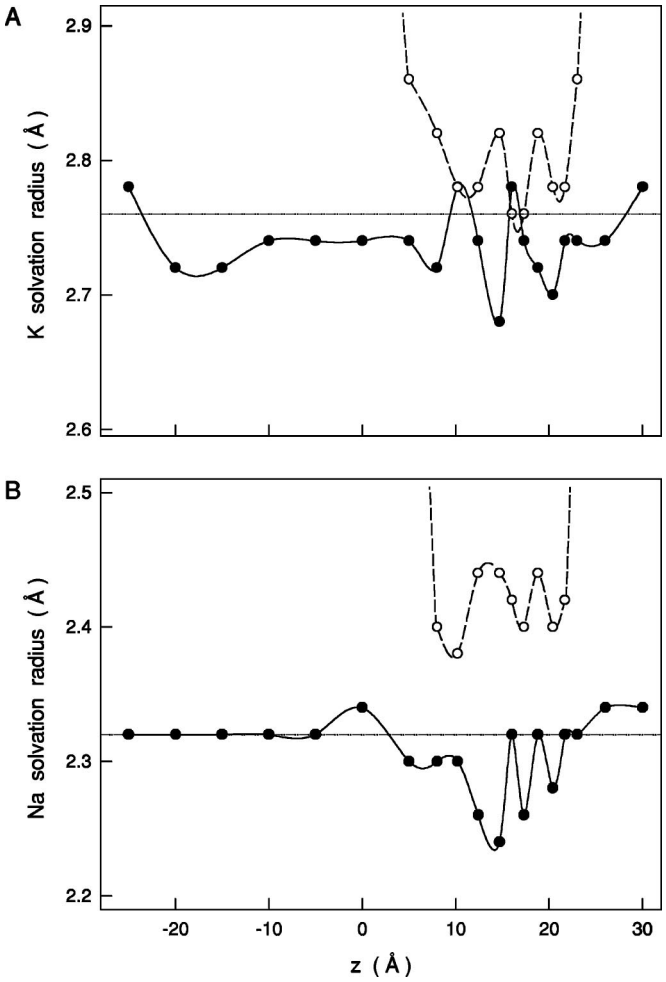

FIG. 7. Solvation radii of K^+ (A) and Na^+ (B) ions: Positions of the first maximum in the RDFs for water oxygen (solid curves, closed circles) and protein oxygen (dashed curves, open circles) are compared to the position of the first maximum in the bulk ion–water RDF (horizontal dash-dot line). Errors are ± 0.04 Å for all values.

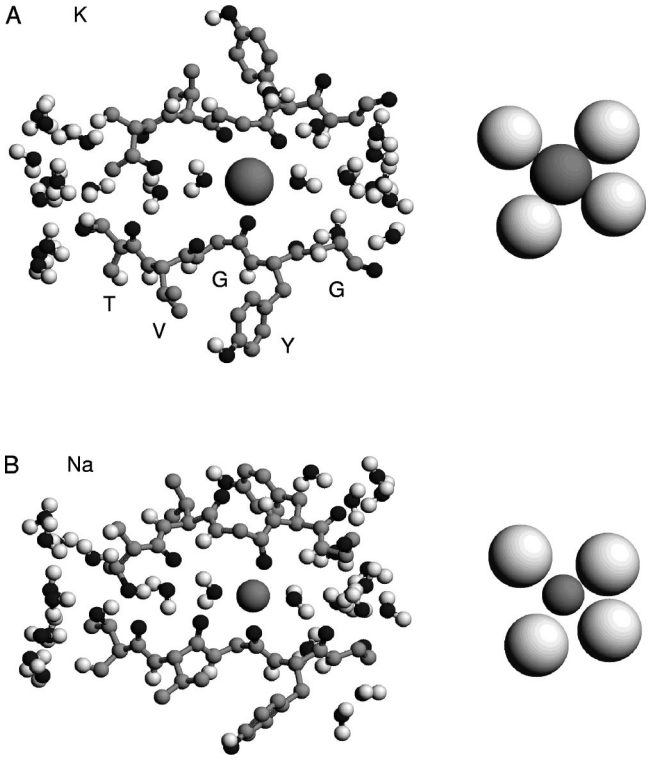

FIG. 8. (A) Sample coordinates for a K^+ ion held near $z=17.3$ Å. The left-hand panel shows an orthogonal view of the protein and water structure at the end of the simulation. Only the selectivity filter segment of the protein (TVGYG where T=threonine, V=valine, G=glycine, and Y=tyrosine) is shown, and only two of the four subunits of the tetramer are drawn. The large gray sphere is the K^+ ion, small black spheres represent oxygen atoms, gray spheres represent carbon and nitrogen atoms, and white spheres represent hydrogens. The right-hand panel of (A) shows the ion-glycine carbonyl oxygen configuration as viewed from along the z axis. Here the gray sphere is the K^+ ion and the white spheres are carbonyl oxygen atoms. (B) Views of the structure in the presence of a Na^+ ion are shown.

Figure 8 illustrates the ability of the selectivity filter to properly solvate K^+, but not Na^+ ions. The left panel of Fig. 8(A) shows a side-on view of a sample of the protein and water structure in the presence of a K^+ ion held near $z=17.3$ Å. The K^+ ion is solvated by two water molecules and six protein (four glycine and two valine carbonyl) oxygen atoms. Two of the four valine carbonyl groups have moved away from the pore, possibly due to the unfavorable interaction they have with the ion's hydrating water mol-

TABLE IV. Bulk ion properties r_{max}, r_{min}, n, and D are the first minimum and maximum in the RDF, the first hydration number and the diffusion coefficient, respectively. D_{self} is the water self-diffusion and τ^{-1} is the first-order inverse rotational correlation time constant of pure water. Simulations involve 528 SPC/E water molecules in a periodic box of side 25.08 Å at temperature 298 K. After 200 steps of steepest descent minimization and 50 ps of heating and equilibration, 100 ps of dynamics is used to determine pure water properties. A single ion is added, removing water molecules within 2.6 Å of the ion center, leaving 525 SPC/E molecules. After 200 minimization steps and 50 ps of heating and equilibration, 500 ps of trajectory data is used to produce bulk ion diffusion estimates. Errors in hydration results are estimated from distribution data while errors in diffusion coefficients are ± 1 standard error of means.

Property	K^+		Na^+
r_{max} (Å)	2.76 ± 0.04 [2.7[a]]		2.32 ± 0.04 [2.4[a]]
r_{min} (Å)	3.65 ± 0.15		3.10 ± 0.08
n	7.2 ± 0.4 [5.5[b]]		5.56 ± 0.03 [4–6[c]]
D (Å^2/ps)	0.14 ± 0.01 [0.1957[d]]		0.09 ± 0.01 [0.133[e]]
D_{self} (Å^2/ps)		0.231 ± 0.006 [0.23[d]]	
τ^{-1} (ps^{-1})		0.19 ± 0.01	

[a]Reference 38.
[b]Reference 39.
[c]Reference 40.
[d]Reference 41.
[e]Reference 42.

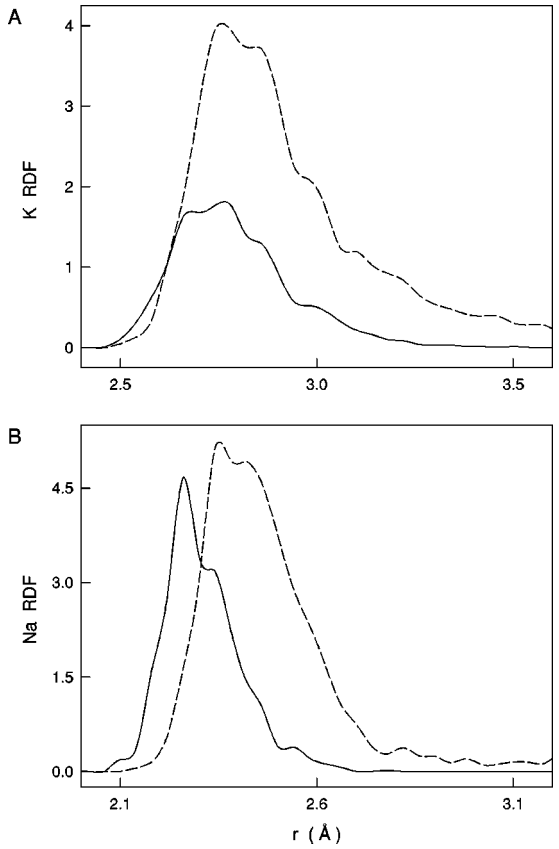

FIG. 9. Radial distribution functions for K^+ (A) and Na^+ (B) ions held near $z=17.3$ Å. Solid curves show the ion–water oxygen RDF while dashed curves show the ion–protein oxygen RDF.

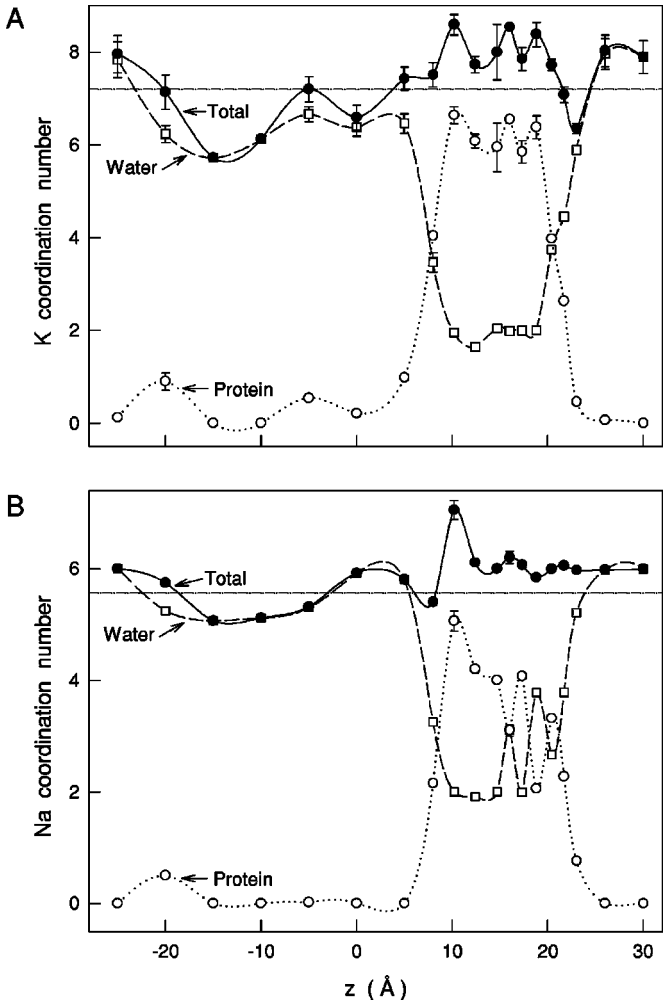

FIG. 10. Solvation numbers of K^+ (A) and Na^+ (B): First water (dashed curves, open squares), protein (dotted curves, open circles), and total (solid curves, closed circles) solvation numbers taken from integrated distribution functions are plotted. The bulk first hydration numbers are drawn as horizontal dash-dot lines.

ecules, lack of space near the ion, or the hydrogen bonding interaction offered by the hydroxyl group on the tyrosine sidechain. We note the obvious flexibility of the protein where one of the two subunits shown has been shifted with respect to the other, helping solvate the ion. This flexibility is in agreement with the experimental findings of Kiss, Lo-Turco, and Korn.[5] The right-hand panel of Fig. 8(A) reveals the close fit with neighboring glycine-carbonyl oxygens. A good fit with the two valine-carbonyl groups also occurs.

Figure 8(B) shows the structure with a Na^+ ion held near $z=17.3$ Å. We note that the flipping of valine-carbonyl groups increases available volume for those water molecules, and is likely to reduce the repulsive electrostatic forces acting between opposite carbonyl groups. The hydrating water molecules would provide obstacles to the inward motion of valine and tyrosine carbonyl groups, and because of strong potentials maintaining the shape of the valine-glycine-tyrosine linkage, their presence could be to some degree responsible for the poor Na^+-carbonyl fit. The right-hand panel of Fig. 8(B) displays the Na^+-glycine carbonyl oxygen arrangement. In order to achieve the bulk coordination number of approximately 6, all four of the glycine oxygens are required within the first shell of the ion. However, in this sample the mean gap of approximately 0.21 Å would lead to an energy barrier. Figure 9 shows the RDFs for K^+ (A) and Na^+ (B) for water and protein oxygens for an ion held near $z=17.3$ Å. This time averaged representation reinforces the view of the poor fitting of the first solvation shell of the Na^+ ion. A similar picture emerges at each position throughout the selectivity filter.

Figure 10 displays the first shell coordination numbers of K^+ (A) and Na^+ (B) ions. Throughout the filter region both ions appear to maintain first solvation numbers equal to or greater than bulk, with just a small loss of less than one oxygen for the K^+ ion at $z=23$ Å. However, both ions show consistent reductions from bulk of their solvation numbers in the narrow hydrophobic pore. The losses for the K^+ ion do not seem to have affected its potential energy adversely in this region, whereas the Na^+ ion has developed a large potential energy barrier (see Fig. 5), illustrating the difficulty the smaller ion faces in attempting to achieve such a large solvation energy. Since protein contributions to K^+ and Na^+ ions in this region are identical (to within errors), they contribute nothing to the observed potential energy margin. The margin arises from poor first shell solvation of the Na^+ ion. The first shell contributions to the K^+ and Na^+ ions at $z=-10$ Å, for example, are -166.6 ± 3.2 and -208.2 ± 4.2 kT, or 6.5 ± 3.6 and 24.0 ± 4.3 kT greater than the reservoir values.

The angle Ψ a water dipole makes with the ion–water vector within the first hydration shell of the ion is given by

$$\Psi = \cos^{-1}\left[\frac{r_{IH}^2 - r_{IO}^2 - r_{OH}^2}{2 r_{IO} r_{OH} \cos\alpha}\right], \quad (1)$$

where r_{IO} and r_{IH} are the positions of the first maxima in the ion–water oxygen and ion–water hydrogen RDFs, respectively, and $r_{OH}=1$ Å and $\alpha=54.74°$ for the SPC/E water model. Variations of up to 45° from the reservoir values have been observed for both ion types near the center of the selectivity filter. Occasionally one water molecule may flip from its natural orientation (negatively charged oxygen atom directed towards cation) as a result of strong hydrogen bonding of the water with the carbonyl groups of the protein. However, the protein appears to be able to compensate by stabilizing the ion with its polar groups. Thus we can see no direct correlation between hydration water orientations and ion potential energy margins within the filter region, and attribute most of the discrimination to the poor fit of protein oxygens within the Na^+ solvation shell.

In summary, toward the center and extracellular side of the filter region where the influence of the pore helix field is reduced, and water contributions to the ion solvation are small, both ions rely strongly on coordination by selectivity filter protein oxygen atoms. The close fit of protein oxygens in the K^+ shell, and the small solvation energy required to stabilize that ion, result in a deep potential energy well. However, when water contributions are limited, Na^+ requires a much larger stabilizing potential from the protein atoms. The carbonyl and hydroxyl groups are unable to provide this amount of energy, and the Na^+ ion experiences a less favorable environment.

IX. FREE ENERGY PERTURBATION

The ability of the channel to discriminate between K^+ and Na^+ ions is best determined by calculation of free energy differences. We employ the free energy perturbation method[43] using the PERT and WHAM facilities of CHARMM. The quantity we calculate

$$\Delta\Delta A_{K^+\to Na^+}(z) = \Delta A_{K^+\to Na^+}(z) - \Delta A_{K^+\to Na^+}(z_0), \quad (2)$$

is the free energy change associated with the creation/annihilation transformation of a K^+ ion into a Na^+ ion with respect to the reservoir reference value at z_0. Each ΔA is an average of forwards and backwards transformations. If the $\Delta\Delta A$ value is positive it means that more energy is required to transform from K^+ to Na^+ within the channel than is required in a bulklike environment, thus indicating that it is less likely for a Na^+ ion to exist at that point than a K^+ ion. Similar calculations have been carried out in the past for the gramicidin channel[44] and a simple model potassium channel.[15] Following equilibration, with an ion constrained at a z coordinate, potential parameters of the K^+ ion are transformed into those of the Na^+ ion in six windows of 20 ps (5 ps equilibration and 15 ps ensemble generation). Reverse transformations begin after equilibration with a Na^+ ion. Free energy perturbation values used for examining the effect of constraints on selectivity (Sec. V) involve longer 50 ps windows (30 ps equilibration and 20 ps ensemble generation).

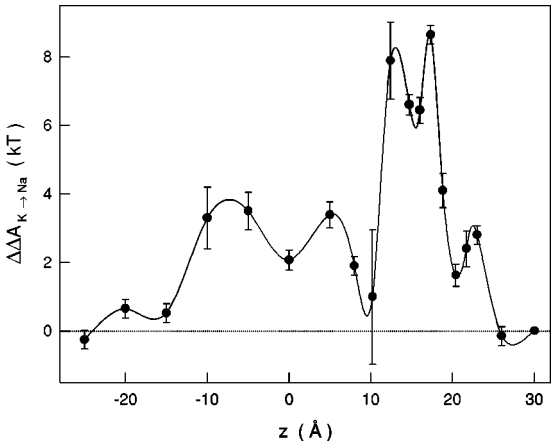

FIG. 11. Free energy perturbation profile: Free energy changes for the transformation $K^+\to Na^+$ with respect to the reservoir ($z=30$ Å) value are plotted. Errors bars represent the hysteresis in each measurement.

Figure 11 shows the free energy perturbation profile throughout the channel. The free energy changes remain positive, or near zero over the entire channel with respect to the extracellular reservoir. The difference is large throughout the selectivity filter, reaching a maximum of 8.6 ± 0.5 kT at $z=17.3$ Å. This free energy difference would correspond, via a Boltzmann factor, to a selectivity margin of 5.4×10^3, complying with experimental evidence of a $\sim10^4$ margin in ion conductances. We note that Fig. 5 appears to support a large margin between Na^+ and K^+ ions in the range $8\leqslant z \leqslant 10.2$ Å due to effective solvation of K^+ by threonine residues near the chamber entrance of the selectivity filter. However, Fig. 11 reveals that only a small margin exists in the free energy. Therefore the greatest ion discrimination arises within the selectivity filter and not within the chamber region, as one may be led to believe from Fig. 5. Also, the large Na^+-K^+ potential energy difference in the narrow hydrophobic pore has not been completely annulled by entropic contributions.

The free energy differences observed here are about half the values obtained with a simple selectivity filter model.[15] In that study, only the filter segment of the protein is employed with harmonic constraints used to mimic all interactions with the remaining structure. The larger free energy difference can be attributed to the reduced flexibility incurred by applying constraints directly to the selectivity filter. Although investigations showed that energies did not change much when constraints were varied, the presence of even quite small constraints applied directly to the filter protein is sufficient to prevent the large deformations seen in this improved channel model. An example of this is the subunit shifting and flipping of carbonyl groups seen in Fig. 8. Nevertheless, the same mechanisms found in Allen, Kuyucak, and Chung[15] hold in this study, and it is only the magnitude of the discrimination that has been reduced.

TABLE V. Pure water properties: Water density (ρ), first-order inverse rotational correlation time constant (τ^{-1}), and self-diffusion coefficients (D_z) are given for the three segments of the channel. The percent bulk values correspond to the axial self-diffusion where bulk values are listed in Table IV. Errors are ± 1 standard error of means.

Segment (Å)	ρ (g/cm^3)	τ^{-1} (ps^{-1})	D_z (Å^2/ps)	% bulk
$8 \leqslant z \leqslant 22$ Å	1.06	0.025 ± 0.009	0.06 ± 0.05	$26 \pm 21\%$
$-2 \leqslant z \leqslant 8$ Å	1.01	0.060 ± 0.007	0.09 ± 0.01	$39 \pm 6\%$
$-20 \leqslant z \leqslant -2$ Å	1.01	0.048 ± 0.008	0.06 ± 0.01	$26 \pm 5\%$

X. WATER PROPERTIES

Water self-diffusion coefficients are calculated by averaging the mean square displacements of water molecules using an overlapped data procedure.[45] We consider the range 0.5–10 ps after the initial shoulder, which corresponds to inertial motion within the hydration cage. Before calculating diffusion coefficients, the center of mass of the system is subtracted to remove any net momentum associated with the periodic boundary. We consider only axial diffusion given by

$$D_z = \frac{1}{2}\frac{d}{dt}\langle [z(t) - z(0)]^2 \rangle. \tag{3}$$

Water rotational correlation is determined by analyzing the decay of the dipole autocorrelation. The dipole autocorrelation function is defined as the time and system average of the cosine of the angle $\chi(\Delta t)$ a water dipole at time $t_0 + \Delta t$ makes with its dipole at time t_0. The sampling procedure for this calculation is identical to that used for diffusion. A mono-exponential decay is justified by analysis of the autocorrelation functions and the inverse rotational correlation time is given by

$$\tau^{-1} = -\frac{d}{dt}\ln\langle \cos \chi(\Delta t) \rangle. \tag{4}$$

Table V includes mean water density, rotational correlation, and self-diffusion estimates for the hydrated potassium channel. Only those waters within the channel pore, having radial position less than the time averaged minimum pore radius, are included in density and diffusion estimates. This excludes molecules embedded in the protein outside the pore. Throughout the entire channel and reservoirs the water density remains approximately the same as bulk. Despite the small dimensions of the long hydrophobic pore, and the hydrophilic nature of the selectivity filter region, self-diffusion remains above 1/4 of bulk self-diffusion throughout the channel.

We compare our results to those for the simple model channel of Allen, Kuyucak, and Chung.[15] Mean axial self-diffusion in the selectivity filter, hydrophobic chamber, and long pore regions of this model channel were ~7%, 71%, and 141% of bulk self-diffusion, respectively. The self-diffusion in the selectivity filter has risen in comparison to the simple model because of increased flexibility of the filter protein. It has fallen in the chamber region because of the less spherical shape and the significant involvement of the –COOH termini of the pore helices, now treated explicitly. The self-diffusion in the long hydrophobic pore has been significantly reduced as a result of narrowing of the pore from minimum radius 3 to ~2 Å in this model, and the presence of wall structure. Reduced water density was also a contributing factor to the enhanced hydrophobic pore diffusion in the simplified model.

It is seen in previous work[10,15] that there is a strong relationship between axial self-diffusion and inverse rotational correlation. Average first-order inverse rotational correlation time constants from the simplified potassium channel model[15] in the selectivity filter, wide chamber, and long pore are approximately 0.005, 0.06 and 0.12 ps^{-1}, respectively. The inverse time constants (Table V) have risen in the filter region and fallen in the hydrophobic segments of the channel in this work for the same reasons the axial self-diffusion was seen to change. The reduction of inverse rotational correlation in the hydrophobic regions is likely to decrease the shielding ability of the water and thus increase electrostatic interactions between ions and protein. In contrast the increase in τ^{-1} in the selectivity filter is likely to cause some shielding of electrostatic forces within that region. We conjecture that this could lead to reduced interaction energies and ion–ion distances within the selectivity filter, altering the preferred multiple ion configurations from those observed by Allen, Kuyucak, and Chung.[15]

XI. MULTIPLE ION CONFIGURATIONS

To investigate multiple ion configurations, two or three K^+ ions are added to the channel at various positions within the selectivity filter and wide hydrophobic chamber, creating configurations similar to those anticipated by experimental data[1] and simple model simulations.[15] A total of 30 simulations, in the absence of any external field, of length 150–200 ps are carried out. The optimum position of a single K^+ ion within the channel would be governed by its free energy profile. Ignoring entropic contributions, the ion potential profile in Fig. 5 suggests that an ion inside the selectivity filter region would prefer to reside near $z = 8-10$ or 16 Å. When initially two ions are placed within the selectivity filter, the mean coordinates after simulation are {10.0, 16.4} Å, while when one ion is placed in the filter and one in the chamber the mean coordinates are {5.0, 15.0} Å. These two configurations are illustrated in Figs. 12(A) and 12(B), respectively.

The potential energy profile of Fig. 5 indicates that the ion near $z = 5$ Å observed, in our second two ion configuration, would prefer to reside near $z = 8-10$ Å due to the presence of a deep well. However, there is evidence, based on the free energy perturbation results of Fig. 11, that the depth of this well may be considerably reduced by entropic contributions. Considering ion–ion repulsion may lead to a preferred $z = 5$ Å equilibrium position. However, we remark on the possibility that there is some obstacle to the passage of an ion from $z = 5$ to 10 Å. Analysis of mean ion radial positions suggests that energy minima for the K^+ ion are considerably off axis in the hydrophobic chamber region (by as much as 2.3 Å). Examination of sample coordinates where a K^+ ion resides near the mean position ($z \approx 5$ and $r \approx 2.3$ Å) reveals that the distances of the ion to carbonyl oxygen atoms on T_{74} and T_{75} residues are 4.68 and 5.38 Å, respectively, while the

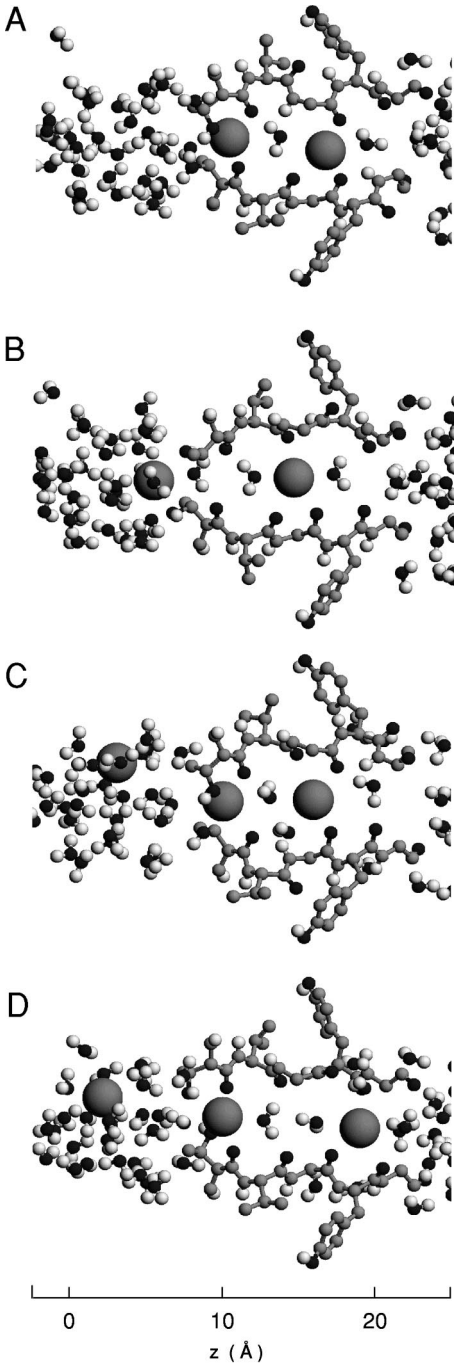

FIG. 12. Multiple ion configurations. Sample coordinates representative of the two most frequently observed two ion (A and B), and three ion (C and D) configurations are shown. The large gray spheres are the K^+ ions, small black spheres represent oxygen atoms, gray spheres represent carbon and nitrogen atoms, and white spheres represent hydrogens.

distances to hydroxyl oxygens on T_{74} and T_{75} are 8.05 and 2.76 Å. Thus, as a result of the flexibility of the protein, the ion appears to bind to the base of the selectivity filter with strong interactions from neighboring residues at the terminus of the pore helix. While this is the case after extended equilibration periods, this binding may be avoided in a conducting channel. Finally we note that a K^+ ion placed beyond $z \approx 19$ Å may be easily ejected from the channel.

Now consider three unconstrained ions placed within the selectivity filter and chamber regions in the absence of applied electric fields. If two ions are placed too close together, especially with one ion near the extracellular entrance, one ion is expelled from the channel. In this case the average positions of the remaining two ions is {3.3, 15.4} Å, a configuration seen in two ion simulations. In no instance is the selectivity filter seen to hold three ions. One ion always resides in the wide chamber region with mean z value 2.0 Å, and two ions in the selectivity filter. Two discrete three ion configurations arise with mean positions {2.0, 9.6, 15.6} and {2.0, 11.4, 19.3} Å as illustrated in Figs. 12(C) and 12(D). From two ion simulations the latter of these two configurations is thought to be fairly unstable.

Experimentally, regions of high ion probability density are seen near the middle of the wide chamber region (z between 0 and 5 Å), a broad peak toward the intracellular side of the selectivity filter adjacent to threonine carbonyl and hydroxyl oxygen atoms (between $z=8$ and 13 Å), and toward the extracellular side of the filter between central glycine and tyrosine carbonyl rings (between $z=18$ and 20 Å). The occurrence of positions 2.0, 9.6, 11.4 and 19.3 Å in our multiple ion simulations is therefore in agreement with experimental findings. The configurations observed here are also in agreement with those seen in simplified channel studies.[15] However, the frequent occurrence of an ion near $z=15-16$ Å in two and three ion configurations is not strongly supported by experiment. Comparison with experiment is made difficult by the low resolution (4.0 Å) of the Rb difference map of Doyle *et al.*[1] However, it is likely that the neutral protein model used here results in a preference for a $z=15-16$ Å position over a $z=18-20$ Å position. In Fig. 3 we see a deep potential energy well in the outer end of the selectivity filter when acidic and basic residues are charged. It is possible that the presence of multiple K^+ ions causes dissociation of these residues, leading to an energy well that increases the propensity for a K^+ ion in the outer region of the selectivity filter. If this were the case then any combination of two or three ion states could reproduce the experimentally determined ion positions. It has been pointed out by Allen, Kuyucak, and Chung[15] that because of the relative instability of the three ion configurations, it is more likely that a combination of two ion states is responsible for experimental ion density maps. However, the possible increased dielectric response of water within the selectivity filter, alluded to in Sec. X, could help stabilize the three ion states. Finally, the idea of having charges created by the presence of multiple ions in the channel is preferable to permanent charges since such stabilizing fields could eliminate a Na^+ energy barrier to conduction in the absence of K^+ ions.

To observe the effect of external fields on ion positions in the chamber and filter regions, a total of 25 simulations of length 400 ps with a strong 7 mV/Å applied field pushing ions outwards or inwards (intracellular–extracellular or extracellular–intracellular) are carried out. In the presence of a strong 7 mV/Å field pushing cations out of the cell, the only two ion configurations seen have mean coordinates {5.3, 12.4} or {5.5, 15.6} Å. With the opposite driving force the only two ion configurations seen are {9.5, 16.0} and {9.6, 19.8} Å. Note that this driving force is not sufficient to push

TABLE VI. Ion diffusion results. Estimates of axial ion diffusion are given for each region of the potassium channel. Errors are ±1 standard error of means.

Ion	Segment (Å)	D_z (Å^2/ps)	% bulk
K^+	$8 \leqslant z \leqslant 22$	0.014±0.003	10±3%
	$-2 \leqslant z \leqslant 8$	0.070±0.008	50±9%
	$-20 \leqslant z \leqslant -2$	0.12±0.07	86±56%
Na^+	$-2 \leqslant z \leqslant 8$	0.015±0.002	17±4%
	$-20 \leqslant z \leqslant -2$	0.03±0.01	37±16%

an ion from the energy minimum near $z=10$ Å into the hydrophobic chamber within 0.4 ns. With three ions maintained in the channel in the presence of an outwards external field the mean configuration is {5.1, 12.3, 18.1} Å.

XII. ION DIFFUSION COEFFICIENTS

Table VI lists mean ionic diffusion values in the three segments of the channel. The results given involve a total of 17 simulations of length 200–400 ps with three ions placed in the channel in the absence of any applied field. Diffusion coefficients in the presence of a strong external electric field are found to be similar and are therefore not reported. Coefficients are calculated using the same procedure as used for water self-diffusion.

In the selectivity filter region 10% of bulk K^+ ion diffusion is observed on average. We note that analysis of ion trajectories reveals that ion motion is governed by Coulomb interactions between ions rather than by diffusive processes. An illustration of this is given by Allen, Kuyucak, and Chung.[15] Brownian dynamics studies[46] have shown that the channel achieves high conductances with diffusion coefficients at this level. We remark that the 12 Å long-range cutoff, although not expected to interfere with ion–ion interactions within the short selectivity filter region, could possibly prevent ions from traversing the entire channel. Thus, if one were to further this current investigation to study channel permeation, alternative treatment of long-range electrostatic forces, such as Ewald summation,[47] may be required.

In the wide hydrophobic region the K^+ ion exhibits around half of its bulk diffusion. In the same region a Na^+ ion experiences only approximately 1/6 of bulk diffusion. However, because multiple ion configurations with the Na^+ ion have not been attempted, this measurement comes from placing a single Na^+ ion in the hydrophobic cavity. Figure 5 shows that, in the absence of Coulomb repulsion by other ions, this ion may be locked in a local energy minimum reducing its mean square displacement.

In a separate set of simulations, a single K^+ or Na^+ ion is placed at one of several positions in the long hydrophobic pore region and a series of 16×200 ps simulations are performed for each ion so as to compute average diffusion coefficients. The operation of the long hydrophobic pore formed by the inner helix is likely to be dependent on its dimension. If the atoms are rigidly held near the initial positions, ions may be unable to traverse the pore. Therefore, when simulating ions in this long narrow region we employ a weaker set of constraints.[32] This permits the region to expand slightly in the presence of a hydrated ion. Diffusion of the K^+ ion varies depending on the position of the ion. When an ion is placed near the wider pocket at $z \approx -15$ Å, little ion translation is observed, whereas an ion placed at $z \approx -10$ Å will quickly move toward the wide chamber region. In fact, diffusion ranges from near zero up to almost four times the bulk value with an average value of 86% of bulk. The fast motion of ions is in agreement with trajectories observed in Brownian dynamics simulations.[46] As a comparison the Na^+ ion shows moderately low diffusion, with around 1/3 of bulk ion diffusion on average throughout the narrow long pore region. Because of the smaller size of the Na^+ ion, it does not experience such large fluctuations in diffusion.

We compare our results for K^+ ions with those found by Allen, Kuyucak, and Chung.[15] In that model the K^+ diffusion remains close to bulk levels (>50%) throughout the hydrophobic pore, and drops to as low as 8% of bulk diffusion in the selectivity filter. We again note that the model channel is as much as 1 Å wider throughout the hydrophobic pore, which should enhance diffusion. However, the simplified model appears to give a reasonable description of K^+ ion diffusion throughout the channel.

Ion diffusion results may also be compared to other model channels. A suitable comparison for the selectivity filter region would be gramicidin A where K^+ ion diffusion ranges between 29% and 49% of experimental bulk.[48] Since the potassium channel selectivity filter is narrower than gramicidin (with radius ~2 Å), our estimate of ~10% of bulk diffusion is in reasonable agreement. The results can also be compared to those for narrow hydrophilic cylinders.[10] A radius 2.1 Å cylinder with a regular molecular wall has mean Na^+ diffusion of around 20% of bulk. A larger K^+ ion in a smaller hydrophilic pore should lead to a smaller diffusion coefficient, and thus there is a consistency between the models.

We make comparison of wide hydrophobic chamber results with a nAChR model channel created by an M2 helix bundle. The pore is as narrow as 6 Å radius and supports 2/3 of bulk Na^+ ion diffusion.[49] This result compares well to the 50% K^+ diffusion observed in the 5 Å hydrophobic chamber. We compare our narrow hydrophobic pore results to those within atomic periodic cylinders[10] of radius 2.1 Å. Na^+ diffusion in this cylindrical channel is approximately 18% of bulk diffusion. While this value is lower, it compares favorably to our result of ~37% for the hydrophobic pore of the potassium channel. Results for a 2 Å exponentially repulsive cylindrical pore[9] show around 15% of bulk Na^+ diffusion, also in fair agreement. Thus our ion diffusion results within all segments of the potassium channel are consistent with the existing estimates from model pores.

Given the high levels of K^+ ion diffusion throughout the hydrophobic regions of the potassium channel, and evidence that 10% diffusion within the selectivity filter does not greatly attenuate conductances,[46] we expect a high throughput of ions within this channel. Ions are observed remaining close to the channel axis in all segments except the wide hydrophobic cavity where a mean radial position of 2.3 Å occurs. However, these mean positions have been generated with a single ion held at the one position for extended peri-

ods. The presence of one or two ions in the selectivity filter may hold the third ion away from the pore helix and selectivity filter –COOH termini (where the ion appears to bind). In fact, three ion configurations show a preference for $z=2$ rather than 5 Å for an ion in the chamber. In this case the ion would reside closer to the axis, primed for its passage into the selectivity filter once a vacancy occurs.

XIII. SUMMARY AND CONCLUSION

Simulations with the entire experimentally determined protein structure of the KcsA potassium channel from *Streptomyces lividans* have been reported. The inclusion of the entire protein has reduced model dependencies in comparison to previous simulations with a simplified model.[15] The model dependencies are limited to the size of constraints applied to the outer regions of the protein to mimic the lipid bilayer, the water model, and the extent of dissociation of acidic and basic sidechains within the protein, each of which has been investigated in this study. A survey of the effect of restraining potentials reveals that, within the regime of weak harmonic constraints on inner and outer helices, the restraining potentials have negligible effect on ion discrimination. Second, comparison of water models shows that TIP3P, and its associated flexible model, are inappropriate for the study of narrow hydrophilic regions such as the selectivity filter. The excellent description of bulk water and ion properties makes SPC/E the obvious water model for this study. Finally, the effect of charged arginine, glutamic acid, and aspartic acid residues on protein contributions to the potential profile has been determined. It is likely that these residues will remain mostly neutral. However there is some evidence of the need for charged sidechains near the extracellular entrance. It is possible that experimentally determined ion densities may only be achieved if an additional deep energy well near the extracellular end of the selectivity filter were created by some of these charged residues. The generation of these charges by dissociation in the presence of multiple ions is the most likely occurrence as this would maintain the Na^+ ion energy barrier in the absence of K^+ ions.

The inclusion of the entire protein leads to considerable flexibility of the selectivity filter, resulting in enhanced water diffusion and rotation. Large motions of carbonyl and hydroxyl groups on the selectivity filter protein have been observed. While these large motions are not required to provide K^+–Na^+ ion discrimination, they do alter the ion–protein–water arrangements and affect the level of ion selectivity. The reduced ion discrimination with this flexible potassium channel model leads to ~ 9 kT free energy difference between K^+ and Na^+ ions (in comparison to 18 kT with the simplified model). The corresponding selectivity margin would be of the order 10^4 as seen experimentally. We remark that measurements of selectivity found with the SPC/E model may be underestimated because of the exaggerated K^+ ion coordination, which reduces relative ion stability within the channel.

The explicit inclusion of the pore helix has provided an absolute measure of the stabilization within the wide chamber region, whereas this was a free parameter in the earlier simplified model. The minimum of the pore helix potential has shifted from near the center of the hydrophobic chamber to the bottom of the filter. This is a result of the explicit treatment of the –COOH terminus on the pore helix and the increased flexibility of the selectivity filter protein. The selectivity filter protein contributes as much to the stabilization of ions in the hydrophobic chamber as does the pore helix.

The shape of the narrow hydrophobic pore is seen to change little after hydration. Even when the inner helix is held by very weak constraints, it remains narrow (radius ~ 2 Å) after extended simulation periods. There is evidence that this may correspond to a closed conduction state.[2,3] Despite the small dimensions of the pore, the K^+ ion remains energetically stable while the Na^+ ion, because of its large solvation energy, is poorly coordinated in this region and experiences destabilization. Thus Na^+ ion would be excluded from the intracellular pore in this current model, and would therefore be unable to block the channel as seen experimentally. This supports the notion of a wider open conduction state.

Finally, ion diffusion within the channel is seen to range from $\sim 10\%$ in the selectivity filter to as high as $\sim 90\%$ in the narrow chamber. These results confirm earlier studies with the simplified potassium channel model. Brownian dynamics simulations[46] have demonstrated that high currents can be achieved with a reduced ion diffusion coefficient in the filter, because the permeation mechanism is governed by the Coulomb repulsion of ions, and not by diffusive processes. The fact that ion diffusion is not reduced to negligible levels supports the high throughputs measured experimentally.

ACKNOWLEDGMENTS

This work was supported by grants from the Australian Research Council and the National Health & Medical Research Council of Australia. All calculations were carried out with the Silicon Graphics Power Challenge and Alpha Cluster of the ANU Supercomputer Facility. We thank Dr. Roger Brown for his help in compiling CHARMM on the Alpha platform.

[1] D. A. Doyle, J. Morais Cabral, R. A. Pfuetzner, A. Kuo, J. M. Gulbis, S. L. Cohen, B. T. Chait, and R. MacKinnon, Science **280**, 69 (1998).
[2] E. Perozo, D. M. Cortes, and L. G. Cuello, Science **285**, 73 (1999).
[3] E. Perozo, D. M. Cortes, and L. G. Cuello, Nat. Struct. Biol. **5**, 459 (1998).
[4] L. G. Cuello, J. G. Romero, D. M. Cortes, and E. Perozo, Biochemistry **37**, 3229 (1998).
[5] L. Kiss, J. LoTurco, and S. J. Korn, Biophys. J. **76**, 253 (1999).
[6] D. Immke, M. Wood, L. Kiss, and S. J. Korn, J. Gen. Physiol. **113**, 819 (1999).
[7] E. M. Oglielska and W. Aldrich, J. Gen. Physiol. **112**, 243 (1998).
[8] M. S. P. Sansom, I. D. Breed, I. D. Kerr, and R. Sankararamakrishnan, Biophys. J. **70**, 693 (1996).
[9] R. M. Lynden-Bell and J. C. Rasaiah, J. Chem. Phys. **105**, 9266 (1996).
[10] T. W. Allen, S. Kuyucak, and S.-H. Chung, J. Chem. Phys. **111**, 7985 (1999).
[11] B. Roux and M. Karplus, Annu. Rev. Biophys. Biomol. Struct. **23**, 731 (1994).
[12] C. Singh, R. Sankararamakrishnan, S. Subramaniam, and E. Jakobsson, Biophys. J. **71**, 2276 (1996).
[13] R. Sankararamakrishnan, C. Adcock, and M. S. P. Sansom, Biophys. J. **71**, 1659 (1996).
[14] D. P. Tieleman and H. J. C. Berendsen, Biophys. J. **74**, 2786 (1998).
[15] T. W. Allen, S. Kuyucak, and S.-H. Chung, Biophys. J. **77**, 2502 (1999).
[16] H. Schrempf, O. Schmidt, R. Kümmerlen, S. Hinnah, D. Müller, M. Bet-

zler, T. Steinkamp, and R. Wagner, EMBO J. **14**, 5170 (1995).
[17] Because terminal groups are not present in experimental coordinates and end points are close to the pore lining, we introduce neutral terminal groups to prevent artificial stabilizing potentials. We employ the acetyl blocking group CH_3-CO- as an N-terminal group, while the amine blocking group CH_3-NH- group acts as a C terminal.
[18] A linear least-squares fit to all α-carbon atoms in the pore helices shows that the pore helix dipole makes an angle of $\sim 41°$ with the z axis, and is directed toward the origin in the hydrophobic chamber.
[19] B. Roux and R. MacKinnon, Science **285**, 100 (1999).
[20] Tests show that an 8 Å Lennard-Jones pore permits water oxygen atom centers to approach no further out than a radius of 7.3 Å. Thus a harmonic potential, with a force constant of 100 kT/Å^2, is turned on at radius 7.3 Å to mimic an 8 Å pore in the reservoirs.
[21] B. R. Brooks, R. E. Bruccoleri, B. D. Olafson, D. J. States, S. Swaminathan, and M. Karplus, J. Comput. Chem. **4**, 187 (1983).
[22] P. J. Steinbach and B. R. Brooks, J. Comput. Chem. **15**, 667 (1994).
[23] G. S. Del Buono, T. S. Cohen, and P. J. Rossky, J. Mol. Liq. **60**, 221 (1994).
[24] L. Perera, U. Essmann, and M. L. Berkowitz, J. Chem. Phys. **102**, 450 (1995).
[25] H. J. C. Berendsen, J. R. Grigera, and T. P. Straatsma, J. Phys. Chem. **91**, 6269 (1987).
[26] B. M. Pettit and P. J. Rossky, J. Chem. Phys. **84**, 5836 (1996).
[27] E. Guàrdia and J. A. Padró, J. Phys. Chem. **94**, 6049 (1990).
[28] K. Heinzinger, Physica B **131**, 196 (1985).
[29] E. Neria, S. Fischer, and M. Karplus, J. Chem. Phys. **105**, 1902 (1996).
[30] A. D. MacKerell, Jr. *et al.*, J. Phys. Chem. B **102**, 3586 (1998).
[31] W. L. Jorgensen, J. Chandrasekhar, J. D. Madura, R. W. Impey, and M. L. Klein, J. Chem. Phys. **79**, 926 (1983).
[32] A weak set of constraints that provides some flexibility to the narrow hydrophobic pore is used for illustration of channel shape in this section, and for measurement of ion diffusion in this region in Sec. XII. Constraints on the α carbons of the outer helix and the extracellular half of the inner helix (residues 80–99) are set to 10 kT/Å^2, and those on the intracellular half of the inner helix (residues 100–119) are set to just 1 kT/Å^2.
[33] G. R. Smith and M. S. P. Sansom, Biophys. J. **73**, 1364 (1997).
[34] T. Lazaridis and M. Karplus, Proteins **35**, 133 (1999).
[35] All ion potential energies are calculated with the 12 Å switched force cutoff.
[36] B. Hille, *Ionic Channels of Excitable Membranes*, 2nd ed. (Sinauer, Sunderland, MA, 1992).
[37] The artificial shift involves simply adding 0.1 Å to every ion–atom distance during the averaging of ion potential energies over time.
[38] G. W. Neilson and J. E. Enderby, Annu. Rep. Prog. Chem., Sect. C: Phys. Chem. **76**, 185 (1979).
[39] G. W. Neilson and N. T. Skipper, Chem. Phys. Lett. **114**, 35 (1985).
[40] S.-B. Zhu and G. W. Robinson, J. Chem. Phys. **97**, 4336 (1992).
[41] *CRC Handbook of Chemistry and Physics*, edited by D. R. Lide (CRC Press, Cleveland, 1994).
[42] H. G. Hertz, in *Water: A Comprehensive Treatise*, Aqueous Solutions of Simple Electrolytes, Vol. 3, edited by F. Franks (Plenum, New York, 1973).
[43] M. Mezei and D. L. Beveridge, Ann. (N.Y.) Acad. Sci. **482**, 1 (1986).
[44] B. Roux and M. Karplus, Biophys. J. **59**, 961 (1991).
[45] D. C. Rapaport, *The Art of Molecular Dynamics Simulation* (Cambridge University Press, Cambridge, 1995).
[46] S.-H. Chung, T. W. Allen, M. Hoyles, and S. Kuyucak, Biophys. J. **77**, 2517 (1999).
[47] M. P. Allen and D. J. Tildesley, *Computer Simulation of Liquids* (Oxford University Press, New York, 1987).
[48] B. Roux and M. Karplus, J. Phys. Chem. **95**, 4856 (1991).
[49] G. R. Smith and M. S. P. Sansom, Biophys. J. **75**, 2767 (1998).